Journal of Colloid and Interface Science 439 (2015) 76–87

Contents lists available at ScienceDirect

Journal of Colloid and Interface Science

www.elsevier.com/locate/jcis

Development and characterization of new enzymatic modified hybrid calcium carbonate microparticles to obtain nano-architectured surfaces for enhanced drug loading

G.A. Islan, M.L. Cacicedo, V.E. Bosio, G.R. Castro *

Nanobiomaterials Laboratory, Institute of Applied Biotechnology (CINDEFI, UNLP-CONICET-CCT La Plata), Department of Chemistry, School of Sciences, Universidad Nacional de La Plata, Calle 47 y115, CP 1900 La Plata, Argentina

ARTICLE INFO

Article history:
Received 23 July 2014
Accepted 9 October 2014
Available online 25 October 2014

Keywords:
Calcium carbonate
Hybrid systems
Alginate
Pectin
Microparticles
Alginate Lyase
Levofloxacin
Drug loading
Controlled release

ABSTRACT

Hypothesis: Biopolymer–$CaCO_3$ hybrid microparticles exposed to hydrolytic enzymes can provide new surface tailorable architectures. Soluble Alginate Lyase hydrolyzed alginate chains exposed on microparticle surface are generating considerable matrix changes. The change of porosity and surface to volume ratio is expected to influence absorption of drugs, thereby affecting controlled release profiles. The developed hybrid system potentially shows interesting properties for lung drug administration.

Experimental: Hybrid microparticles were developed by colloidal co-precipitation of $CaCO_3$ in presence of biopolymers: alginate (Alg) or Alg–High Methoxylated Pectin (HMP), followed by treatment with Alginate Lyase (AL). Surface architectures were observed by SEM. The increase in area to volume ratio was confirmed by BET isotherms. Also, enzymatic changes were elucidated by biophysical methods (EDAX, DSC, FTIR, XRD) and determination of the total carbohydrates content. Levofloxacin (a fluoroquinolone antibiotic) as model drug was incorporated by absorption. The drug release profile and the antimicrobial activity of the microparticles were tested against *Pseudomonas aeruginosa*.

Findings: After enzyme treatment, microspheres showed 4 μm diameter and increased porosity. While $CaCO_3$–Alg microspheres resulted in a rougher surface, $CaCO_3$–Alg–HMP ones exhibited "nano-balloon" patterns on surface. Both AL-treated microparticles showed up to 3 and 7 times higher Levofloxacin encapsulation than no treated ones. Microparticles showed controlled drug release profiles and enhanced antimicrobial effect. The present work demonstrates a significant progress in the development of new carriers with potential application for lung infections treatment.

1. Introduction

Calcium carbonate ($CaCO_3$) is one of the most abundant existing minerals in the nature and an important material in the industrial and pharmaceutical fields. Six different polymorphisms of $CaCO_3$ have been reported, but vaterite is the most interesting for microparticles production. Vaterite particles can be synthesized at laboratory scale by two methods: supercritical and chemical synthesis. They showed a spherical geometry with a small crystal size and narrow distribution [1]. Besides size parameters, porous is another special feature to consider in particles formation, as they provide unique properties like enhanced drug absorption and release kinetics, in addition to large surface to volume ratio and low density [2].

These properties make $CaCO_3$ microparticles attractive carriers for pulmonary delivery, as they are inert material and provide sizes around 5 μm that are suitable for nasal administration [3]. It has been demonstrated that particles larger than 5 μm mainly accumulate in the periphery of the lung and escaped through phagocytic clearance mechanisms [4]. Furthermore, pulmonary delivery showed some advantages in comparison with other administration ways. The drug is directly administered in the affected lung and local drug concentration could be easily manipulated by the dose. In the case of lung infections treatments, not only the bacterial killing is enhanced, but also the proliferation of resistant microorganisms is reduced [5]. Inhaled microparticles are effective therapeutic carriers for non-invasive systemic delivery of drugs. They can offer

Abbreviations: AL, Alginate Lyase; Alg, alginate; BET, Brunauer Emmett Teller; BJH, Barrett Joyener Halenda; HMP, High Methoxylated Pectin; DSC, differential scanning calorimetry; EDAX, energy dispersive X-ray spectrometry; FTIR, Fourier transformed infrared spectroscopy; HMP, High Methoxylated Pectin, Levo, Levofloxacin; LMP, low methoxylated pectin; MMP, medium methoxylated pectin; SEM, scanning electron microscopy; XRD, X-ray diffraction.

* Corresponding author. Fax: +54 221 483 37 94 103.
E-mail address: grcastro@gmail.com (G.R. Castro).

http://dx.doi.org/10.1016/j.jcis.2014.10.007
0021-9797/

a controlled release profile of the drug, prolonging the airways residence time in the lungs and decreasing the dosage and drug side effects in patients. Some reports, describe $CaCO_3$ systems as useful carriers for intranasal delivery of insulin and hydrophilic compounds, because of their easy production and slow biodegradability [3,6–7].

However, $CaCO_3$ matrices showed some limitations in drug delivery, such as stability in physiological environments and low drug encapsulation efficiency. Drugs or bioactive molecules were adsorbed mainly on the surface of the solid $CaCO_3$ particles. As a consequence, the binding of the adsorbed drug to $CaCO_3$ matrix was not strong enough resulting in an insufficient sustained release or targeting [8].

For these reasons, hybrid microparticles become an innovative alternative to overcome their limitations [9]. Aqueous mixtures of biopolymers and $CaCO_3$ under controlled colloidal precipitation conditions produce hybrid particles displaying molecular sustained release properties, biocompatible design and versatility of the matrix [10–11].

In this scenario, alginate and pectins were selected due to their desirable properties for medical applications, such as biocompatibility, lack of toxicity of their degradation products and no immunogenic response. Alginates (Alg) are linear polysaccharides composed of β-manuronic (M) acid and α-guluronic (G) acid linked by 1–4 bounds. They can be easy crosslinked in presence of divalent ions making hydrogels by the so called "egg box junctions" [12]. Pectins are built of linear polysaccharides of partially methoxylated poly[α-(1,4)-D-galacturonic acids]. They showed different esterification degrees (ED) and they are classified in three main groups: low-methoxylated (LMP) with ED < 40%; medium-methoxylated (MMP) with ED between 40% and 60%; and high-methoxylated pectins (HMPs) with ED > 60%. Pectins can be gelled by multivalent cations or at acidic pHs [13].

Considering that hybrid biopolymeric microparticles could be easily tailoring by taking into account the chemical composition, a biocatalyst modification was proposed. The use of hydrolytic enzymes with specific activity on their natural substrates could play a major role in providing novel architectures with new properties and capabilities. Changes in porosity, surface patterns and biogel network directly impact on the particle structure and properties. Consequently, the loading efficiency and release of molecules carried as cargo by the microparticles can be tailored [14–15].

Among the biopolymeric hydrolases, Alginate Lyase (AL) was selected as the enzyme to modify the hybrid matrices. The AL is depolymerizing enzyme acting over mannuronate or guluronate residues of alginate via beta-elimination mechanism [15–16]. In addition, it was reported that AL is capable to be active on gelled forms of alginate [17]. However, alginate lyase is unable to hydrolyze pectins composed only by galacturonic residues, reason why its use in alginate–pectin blends could allow to establish a specific tailoring of hybrid particles.

Based on the developed matrices and the purpose modifications, the adsorption of a model drug was proposed. Levofloxacin was a candidate, considering its broad spectrum against pathogens and its application in the treatment of bacterial respiratory infections. An early stage of aggressive antibiotic therapy is essential for preventing bacterial establishment and the consequent biofilm formation. In particular, Levofloxacin is commonly used in treatment of many bacterial infections, including respiratory, urinary tract, gastrointestinal, and abdominal infections. Also, Levofloxacin is considered the safest among the fluoroquinolones, with a low rate of hepatic abnormalities [18]. However, common side effects of the drug are affecting the gastrointestinal tract and other organs producing nausea or vomiting, diarrhea, headache, and constipation. Also, the alteration of the normal flora from the colon usually produces pseudomembranous colitis [19]. Due to these undesirable side effects, a controlled release of the drug is a relevant aspect to be considered. In this sense, the use of the $CaCO_3$ hybrid particles as vehicles for the safe administration of Levo via inhalatory therapy could be a feasible therapeutic alternative in the future. Also, an understanding of the mechanism involved in the enzymatic modifications of the hybrid matrices could bring new avenues for the production of novel engineered materials with potential biomedical applications.

The aim of the present work is to develop and characterize hybrid biopolymer–$CaCO_3$ microparticles enzymatically treated with Alginate lyase, displaying innovative mixed gel surface architectures with a desirable size in a narrow distribution. Levofloxacin was used as a drug model to study the loading and extended release for potential application in pulmonary drug delivery. The changes produced by the enzymatic treatment were analyzed by SEM, EDAX, FTIR, XRD, nitrogen adsorption isotherms and DSC studies. The effect of Levofloxacin loading and drug release from microparticles is also discussed. Finally, the antibacterial capacity of the hybrid microparticles containing Levofloxacin was tested against *Pseudomonas aeruginosa*.

2. Experimental

Levofloxacin (Levo, (*S*)-9-fluoro-2,3-dihydro-3-methyl-10-(4-methylpiperazin-1-yl)-7-oxo-7*H*-pyrido[*1,2,3-de*]-1,4-benzoxazine-6-carboxylic acid), apple pectin (DE: 70–75%), Glycine (Gly) and Alginate Lyase (AL) from *Flavobacterium multivorum* able to degrade poly(G) and poly(M/G) [16] were provided by Sigma–Aldrich (cat # A-6973, Buenos Aires, Argentina). Sodium Alginate (MW_{av} = 120 kDa) was purchased from Monsanto (Buenos Aires, Argentina). *P. aeruginosa* ATCC 15442 was used in all experiments. Other reagents were of analytical grade from commercially available sources and used as received from Merck (Darmstad, Germany) or similar brand.

2.1. Synthesis of hybrid calcium carbonate/biopolymer microparticles

Hybrid microparticles were synthesized by colloidal crystallization of $CaCO_3$, in presence of Glycine (Gly) buffer and biopolymers: alginate or high methoxyl pectin (HMP) as previously reported [20]. Briefly, 9.0 ml of an aqueous solution of Na_2CO_3 (3.2% w/v) prepared in miliQ water were mixed with 2 ml of the biopolymeric solution of alginate or alginate/HMP at 1.0% (w/v). Then, 9.0 ml of 3.2% (w/v) of $CaCl_2$ in Gly buffer (pH = 10.0) were added and stirred at 1000 rpm in an ice bath for 5 min. The precipitated products were collected by centrifugation at 10,000*g* for 10 min. The resulting precipitate was washed with miliQ water. Later, the samples were resuspended in water, freeze with liquid N_2 and lyophilized. Finally, the obtained light powder was stored in vacuum desiccators at room temperature until further use.

2.2. Modification of microparticles by Alginate Lyase treatment

A mass of 25 mg of hybrid microparticles was weighted and incubated with 1.5 ml of Alginate Lyase solution (1.0 mg/ml; 40 EU/ml in 25 mM phosphate buffer mM, pH = 7.4) at 37 °C for 48 h. Then, microparticles were washed twice with miliQ water and lyophilized. Controls without enzyme were done.

The AL activity was measured by the detection of oligomeric unsaturated residues produced per minute at 37 °C. The rate of double-bond product formation was assayed using 4600 M^{-1} cm^{-1} molar absorptivity at 233 nm by continuous recording in an UV–visible spectrophotometer as previously reported [21]. The degradation rate of AL on $CaCO_3$/Alg and $CaCO_3$/Alg–HMP microparticles

was established considering the slope of the first points of the product vs. time curve.

2.3. Determination of total biopolymer content

In order to determine the amount of biopolymer into the microparticles after synthesis and AL treatment, the total carbohydrates content was quantified by the anthrone method [22]. Briefly, 10.0 mg of each formulation were completely dissolved in 2.0 ml of 3.0 M HCl solution. The samples were diluted and incubated with the anthrone reagent (in 75% (v/v) H_2SO_4) under a 100 °C for ten minutes. Then, the reaction mixture was cooling down on ice bath and the absorbance at 625 nm was measured. Finally, the data was correlated with an alginate calibration curve.

2.4. Differential scanning calorimetry (DSC) analysis

The DSC profile of the samples was obtained using a TA-Instrument DSC Q2000. Briefly, 5.0 mg of lyophilized powder were placed in a standard aluminum pan, hermetically closed and heated at a constant rate of 10 °C/min from room temperature to 225 °C, under 20 ml/min of nitrogen purging. All samples were run in duplicate.

2.5. X-ray diffraction (XRD)

Analytical Expert Instrument equipped with an X-ray generator (λ = 0.154 nm) was used to characterize the crystalline structure of the microparticles. Samples were scanned in 2θ ranges varying from 2° to 50° (2°/min). Quantitative analysis of the XRD data was performed by using the Scherrer equation to estimate the average crystallite size (D) of the calcium carbonate phase. The equation is described as follows:

$$D = \frac{K.\lambda}{B.\cos\theta}$$

where K is a shape factor (with a value around 1.0) and B the peak width at the half-maximum peak.

2.6. Fourier transformed infrared spectroscopy (FTIR)

The FTIR spectra of the lyophilized samples were directly recorded in a Thermo Scientific Nicolet 6700 spectrometer, with a resolution of 4 cm^{-1}. A number of 32 scans were performed for each sample in the range of 600–4000 cm^{-1}. The ATR (Attenuated Total Reflectance) accessory was utilized in all measurements in order to preserve the microparticles structural integrity.

2.7. Scanning electron microscopy (SEM) images

SEM analysis was carried out in freeze-dried microparticles. Samples were prepared by sputtering the surface with gold using (Balzers SCD 030 metalizer) obtaining layer thickness between 15 and 20 nm. Microparticles surfaces and morphologies were observed using Philips SEM 505 model (Rochester, USA), and processed by an image digitalizer program (Soft Imaging System ADDA II (SIS)).

2.8. Size distribution

The microparticles average size was determined from SEM images at 500× magnifications and processed with ImageJ software (NIH, USA). After setting the scale, the diameter of microparticles (n = 100) was measured and the mean was calculated.

2.9. Roughness analysis

SEM images of microparticles were analyzed by ImageJ software (NIH, USA). The roughness of the surface was reflected by the standard variation of the gray values from the pixels corresponding to each microparticle at 5000× magnification. The less the standard variation value is, the smoother the surface is. In this sense, histograms and plot profiles were obtained.

2.10. Nitrogen adsorption isotherms

Nitrogen adsorption–desorption at 77 K in a bath Temperature of −195.800 °C was carried out for dry microparticles. Surface area, pore volume and pore size of the different formulation were calculated with the Micromeritics ASAP 2020V3.00 Software considering the Brunauer Emmett Teller (BET) equation or the Barrett Joyener Halenda (BJH) method.

2.11. Levofloxacin loading

Levofloxacin (Levo) was incorporated by absorption mechanism. 25 mg of dry microparticles were immersed in 1 ml of Levofloxacin solution (1 mg/ml) and incubated at 5 °C under carrousel agitation for 24 h. After loading, microparticles were separated by centrifugation at 10,000g for 5 min and washed with miliQ water. The supernatant and the washing water were hundred times diluted and not incorporated Levo was spectrophotometrically determined at 286 nm. The maximum loading of microparticles was calculated by two methods: (a) by the difference between the amount of drug initially placed into the starting solution in contact with the microparticles and the amount of remain Levo in solution after the microparticles loading procedure; (b) by total dissolution of microparticles under acid pH (1.0 M HCl), followed by UV detection of Levofloxacin. The UV signal was correlated with a calibration curve of Levo at different concentrations (μg/ml).

2.12. Release of Levofloxacin from microparticles

Levofloxacin loaded microparticles (25.0 mg) were incubated in 1.0 ml of physiological solution (pH = 7.0) at 37 °C. Samples of 0.50 ml were taken out at different times for 24 h and the Levo release was followed by UV detection at the maximum wavelength of the drug (λ_{max} = 286 nm) under our experimental conditions. Finally, 0.50 ml of fresh media was added back to maintain the volume constant, simulating the dynamic conditions during pulmonary drug delivery.

2.13. Optical and fluorescent microscopy

Optical and fluorescence microscopy observations of the Levofloxacin loaded microparticles were performed in a Leica DM 2500 microscope (Germany) equipped with UV filters (495–505 nm).

2.14. Microbiological assay

P. aeruginosa. ATCC 15442 was cultured in nutrient broth medium and incubated at 37 °C for 12 h. An aliquot (1.0 ml) of the growth media was added to 70.0 ml of fresh nutrient broth medium to initiate the culture at 37 °C. After 5 h of incubation, when bacteria were reaching the half exponential phase, 25.0 mg of Levofloxacin loaded microparticles were added. The final inhibition point was determined after 24 h incubation. The bacterial inhibition growth was measured by optical density at 600 nm and the bacterial survival was estimated by UFC/ml count on agar plates.

Photos of each bath were taken in order to elucidate production of the characteristic mucoid green biopolymer by *P. aeruginosa*. Controls of bacterial growth in absence of Levo, with increasing free antibiotic concentrations (from 0.5 to 3.0 μg/ml) and with unloaded antibiotic microparticles were performed.

2.15. Statistical analysis

Experiments were carried out in triplicates. Comparisons of the means were performed by analysis of variance (ANOVA) with a significance level of 5.0% ($p < 0.05$) followed by Fisher's least significant difference test at a $p < 0.05$.

3. Results and discussion

3.1. Synthesis of $CaCO_3$ hybrid microparticles and enzymatic treatment

Colloidal precipitation of $CaCO_3$ in the presence of alginate or alginate/high methoxyl pectin resulted in hybrid microparticles which, after lyophilization process, were obtained as a fine powder. In order to determine the amount of biopolymer into the hybrid microparticles and after AL treatment, the total carbohydrates content was quantified by the anthrone method. The results of the total sugar analysis are shown in Table 1. Synthesis of the hybrid microparticles in the presence of 0.1% (w/v) of total biopolymer brings 24% of carbohydrates content in matrix, independent of biopolymeric sources used in the microparticle synthesis. However, changes in the composition were observed after AL treatment. The $CaCO_3$/Alg microparticles showed a biopolymeric content reduction of 72% meanwhile the decrease in carbohydrate content in the $CaCO_3$/Alg–HMP microparticles was only 28% after enzymatic treatment.

In order to elucidate the relevance of the hydrolytic activity of the alginate lyase in the hybrid particles, the rate of microparticle degradation was analyzed. The alginate degradation rate of the $CaCO_3$/Alg and $CaCO_3$/Alg–HMP microparticles incubated with AL (1.0 mg/ml; 40 EU/ml) was 26.96 and 13.04 μM/h respectively (ESI, Fig. 1S). These results are suggesting that alginate is more accessible for the enzymatic degradation in the $CaCO_3$/Alg formulation compared with the hybrid microparticles containing also HMPectin. The decrease of enzymatic degradation rate in almost a half can be attributed to not only a decrease of the alginate content in the microaparticles but also a steric hindrance of AL because of the differences in the complex polymer formation and chain entanglement in presence of calcium produced by the interaction between HMPectin and alginate. Particularly, the alginate lyase from *F. multivorum* used in our work is an endotype poly G-type lyase cleaving only the linkage between contiguous guluronic units present only in alginate [16]. On the other side, pectins are made mostly of galacturonic units with several degree of methoxylation, but nor guluronic acid and neither mannuronic acid are present in the pectin polymer structure, and linkages are not recognized by the AL [23].

Table 1
Composition of microparticles in terms of biopolymer/matrix ratio determined by total sugars method.

Microparticles	Composition (%) (biopolymer/matrix ratio)
$CaCO_3$/Alg	23.5 ± 3.1
$CaCO_3$/Alg + AL treated	6.5 ± 0.1
$CaCO_3$/Alg–HMP	23.6 ± 1.5
$CaCO_3$/Alg–HMP + AL treated	17.1 ± 3.9

3.2. Characterization of enzymatic modified $CaCO_3$ hybrid microparticles

The analysis of $CaCO_3$/Alg microparticles by DSC showed an endothermic peak at 90.59 °C during heating (ESI, Fig. 2S). This peak corresponds to the dehydration of calcium carbonate structure, which refers to the water molecules intrinsically associated within the matrix. If an integration of this peak is carried out and normalized with the amount of water loss, values close to the vaporization enthalpy of liquid water at 100 °C (40.87 kJ/mol) were detected as it was previously reported [24]. After AL treatment, microparticles showed a decrease shift of 3.5 °C in the peak value, indicating the presence of a more labile structure and/or porous architecture, reason why water molecules are more exposed and prone to migrate out of the matrix. This is reasonable considering the capability of the AL to remove alginate crosslinked chains from the hybrid $CaCO_3$ microparticles, thus modifying their structure. In a similar profile, it was observed an endothermic peak at 95.27 °C for $CaCO_3$/Alg–HMP microparticles. A lower decrease in peak temperature (around 1 °C) after AL treatment was observed. Although a possible modification of the matrix is suggested, the changes are less pronounced than $CaCO_3$/Alg microparticles as it was expected considering the lower content of alginate in the microparticles containing also pectin.

The microparticle polymorphisms of $CaCO_3$ were evaluated by the X-ray diffraction patterns of the different hybrid $CaCO_3$ microspheres treated or not with AL (Fig. 1). The observed peaks typically showed the characteristic $CaCO_3$ vaterite polymorphism. The presence of the peak at 29.3 in the X-ray diffractogram of $CaCO_3$ microparticles was attributed to the most intense peak of calcite. However, this peak was not seen in the diffractograms of the hybrid systems, probably due to the presence of biopolymers which are acting as a template improving the stability of the vaterite crystals, as previously reported [20]. An interesting observation is that AL treatment can modify the X-ray profile of microparticles (Fig. 1 c and e). In the treated hybrid systems, the characteristic vaterite peak at 25 was accompanied by the presence

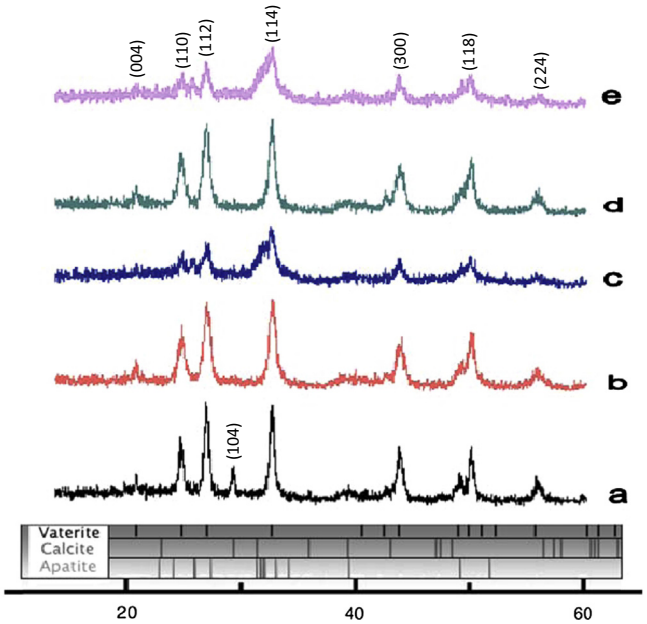

Fig. 1. X-ray diffraction pattern of microparticles: (a) $CaCO_3$; (b) $CaCO_3$/Alg; (c) $CaCO_3$/Alg + AL; (d) $CaCO_3$/Alg–HMP; $CaCO_3$/Alg–HMP + AL. Representative bragg reflexions of vaterite, calcite and apatite X-ray diffractogram ICSD 15879) are indicated with vertical markers below the profiles.

of a peak at 26 in both cases ($CaCO_3$/Alg and $CaCO_3$/Alg–HMP AL treated). Also, near the characteristic peak of vaterite at 33 another peak at 32 had appeared. To explain the presence of new peaks, a comparison with the apatite diffractogram was carried out in terms to evaluate the presence of apatite crystals in the samples. Behind this study emerged the speculation that phosphate ions present in the buffer solution would be feeding the formation of this crystal structure [25]. Characteristic apatite peaks at 26 and 32 of apatite can provide an insight to estimate the formation of new apatite crystals, at least on the surface of the treated hybrid microspheres. Additionally, a decrease in the intensity of the other vaterite peaks was observed when AL treatment was carried out, as the time that new possible apatite peaks appeared. In another deep study, the average crystallite size of the calcium carbonate phase was calculated by analysis of the XRD data using the Scherrer equation. Application of the Scherrer equation can be performed considering: the measurement of the *B* value, subtraction of the instrumental broadening and that all remaining broadening is caused by particle size effects alone. It is important to establish that the Scherrer equation could provide an underestimation of the size values if lattice strains are present in the sample, which often occurs when crystals are co-precipitated in the presence of additives [26]. In the present work, the crystalline size of $CaCO_3$ particles was 15.3 nm for the crystalline planes 110/114 of vaterite and seemed to be uniformly distributed. The calculated domain value was half in size compared to crystalline $CaCO_3$ previously reported [27]. This discrepancy could be probably attributed to the differences in the experimental precipitation procedures. Also, these spectra can differ from those obtained from starting with pure $CaCO_3$. Colloidal precipitation of $CaCO_3$ in presence of alginate and alginate/HMP gave rise to crystals of 10.2/13.1 nm and 11.5/13.1 nm for the 110 and 114 reflections. The reduction in the crystalline size could be attributed to the preferential adsorption of the biopolymer in particular crystal planes. In general, the sizes estimated for the 110 plane are generally smaller than those for the 114 and is indicating that greater lattice strain have been produced in that direction [26]. On the other hand, the values for AL treated microparticles were 9.2/11.5 nm for the 110/114 reflections, indicating that other contributions to the lattice strain appeared and can be endorsed to the apatite deposition on microparticles surface.

Vibrational spectra of the hybrid microspheres are displayed in Fig. 2. Typical FTIR bands associated to the calcium carbonate microspheres structure can be found. In all formulations, the peak associated to vaterite at 744 cm^{-1} was observed, indicating that this is the predominant polymorph structure of calcium carbonate and no conversion to other polymorphism was produced [25]. In $CaCO_3$/Alg microspheres, the band at 1037 cm^{-1} was assigned to the –OH bending of alginate [28]. Furthermore, the region between 1081 and 1024 cm^{-1} was previously assigned to the bending of τ(CO), δ(CCO), δ(CC) and also to the ν_{as}(COC) vibrational modes of alginate [29]. This result is confirming the presence of alginate incorporated into $CaCO_3$ structure, making a new hybrid material. The peak at about 1396 cm^{-1} of calcium carbonate showed a shift to 1385 cm^{-1}, indicating the presence of some type of interactions between the biopolymer and the $CaCO_3$ matrix. However, after treatment of $CaCO_3$/Alg microparticles with AL, a bathochromic shift of the peak to 1398 cm^{-1} was observed and very close to the initial wavenumber of calcium carbonate. This is reasonable considering the enzymatic treatment with alginate lyase which is capable to modify the morphology of the microparticles, displaying "hairy" structures by partial degradation of alginate on the microparticle surface, and allowing to detect again the $CaCO_3$ signal originated from inside of the microparticle. On the other side, a new and intense peak appeared at 1022 cm^{-1} and can be associated with the degradation products made by alginate lyase hydrolysis.

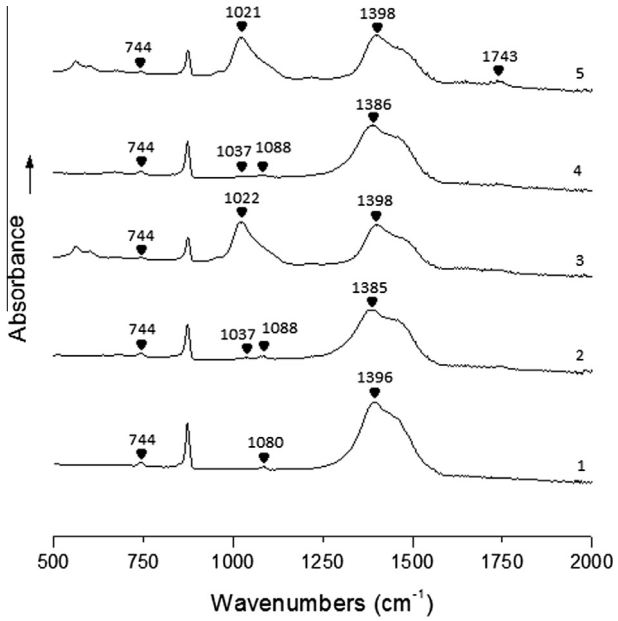

Fig. 2. FTIR spectra of microparticles of (1) $CaCO_3$; (2) $CaCO_3$/Alg; (3) $CaCO_3$/Alg + AL; (4) $CaCO_3$/Alg–HMP; (5) $CaCO_3$/Alg–HMP + AL microparticles.

This band could be associated to the –OH bending band of polyguluronic chains of alginate, after enzymatic removing of mannuronic residues as previously reported [28]. The results are suggesting the partial removal of alginate chains from the hybrid material surface and a modification of its interaction within the matrix. In the hybrid Alg–HMP microspheres, a similar behavior was observed. A shift in the peak of calcium carbonate was found and also the return close to the initial band of $CaCO_3$ after AL treatment. Similarly, the appearance of a peak at 1021 cm^{-1} was observed. But in this case, considering that only alginate chains were removed, the concentration of HMP into the matrix was expected to be increased and that was exactly found by the rise in the intensity of a band at 1743 cm^{-1}. This band is produced by the stretching vibration mode of the methyl ester groups of the HMP.

The SEM micrographs shown in Figs. 3 and 4 provide convincing evidence for the differential action of the alginate lyase on hybrid microparticles. Images of $CaCO_3$/Alg microparticles revealed spherical shapes and smooth surfaces (Fig. 3, left) in a narrow size dispersion (ESI, Fig. 3S). However, strong changes on microparticle surface were observed after treatment with Alginate Lyase (Fig. 3, right). Besides the spherical shape was conserved, new distinctive surface patterns appeared. A rougher surface architecture was evidenced and pores seemed to be distributed in the whole surface. This microparticles re-architecture is indicating a crucial rol of the enzyme by hydrolyzing the alginate covering the surface of the microspheres and perhaps some alginate chains close to the surface. An estimative calculation of the AL dimensions using the equation reported by Erikson [30], considering the molecular weight of 120 kDa and the globular enzyme structure [31], resulted in a mean volume of 145.4 nm^3. Taking into account this value, the hydrolysis of alginate chains inside the microparticles would be unlikely and could be only produced in the microparticles surface. In this sense, $CaCO_3$/Alg microparticles treated with AL are exposing a surface with new holes previously occupied by the alginate chains, creating an interesting pattern with an increase surface to volume ratio. The AL could degrade the alginate in the $CaCO_3$ matrix producing two events: first, the increase of porosity and second, a more available surface for deposition of calcium phosphate from the phosphate buffer. This hypothesis explains the

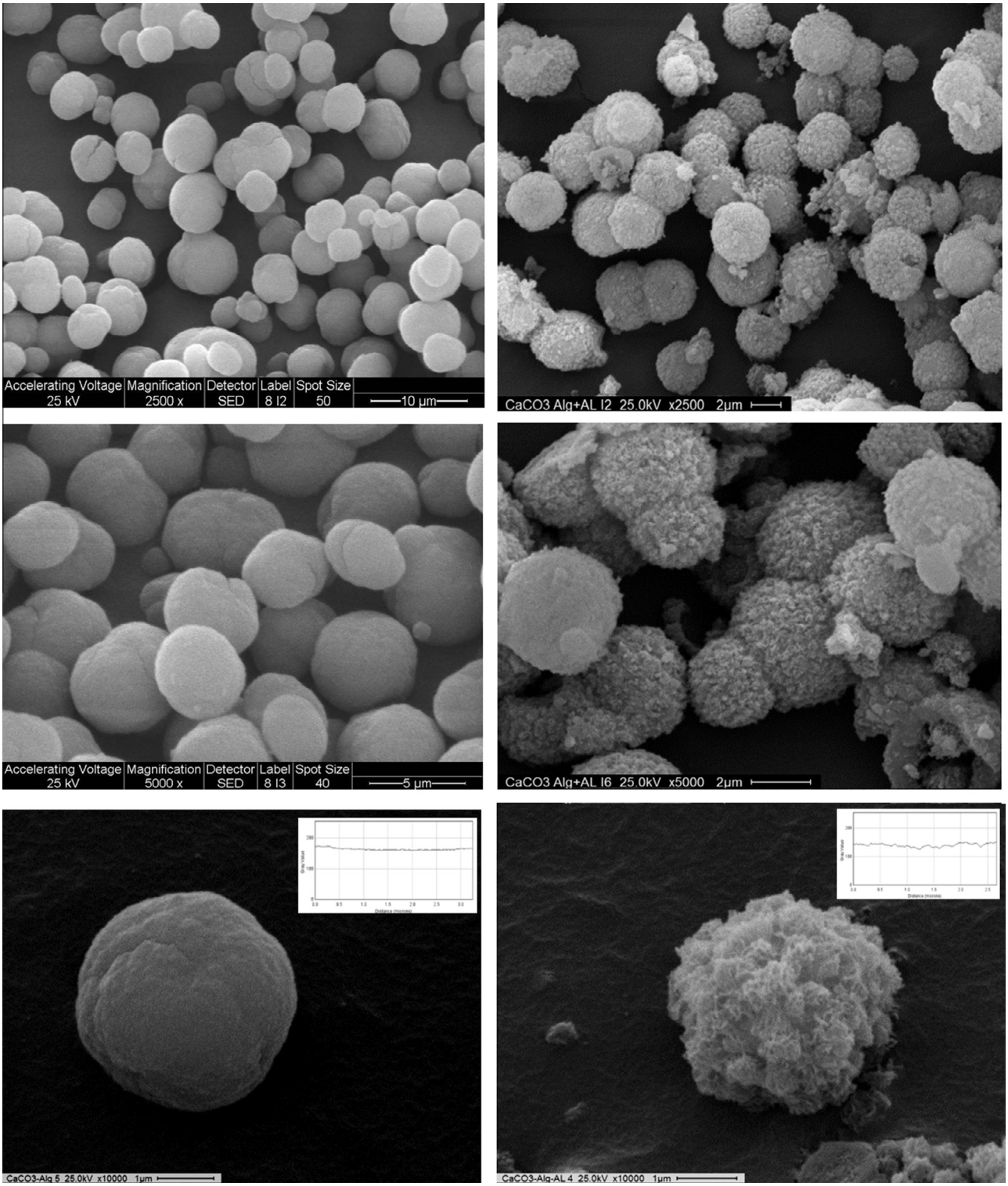

Fig. 3. SEM images of $CaCO_3$/Alg microparticles at 2500× (up), 5000× (middle) and 10,000× (below) magnifications. Left: no treated. Right: Alginate Lyase treated microparticles. The plot profile of microsphere surface is shown in the corner of the bottom images.

appearance of apatite peaks on treated hybrid microspheres. The results are attractive for lung delivery since the presence of more porous and low density particles are relevant tools to guarantee the proper microsphere delivery by aerosolization.

In the same way, significant changes in surface were observed for $CaCO_3$/Alg–HMP microparticles after AL treatment (Fig. 4). While the $CaCO_3$/Alg–HMP microparticles exhibited a smooth surface, the AL treated microparticles showed some "*nano-balloon*" like patterns on surface. The "patches" observed by SEM are probably the regions covered by HMPectin chains in the surface. The alginate zones were removed by the enzymatic hydrolysis of AL meanwhile the HMP remains un-attacked by the enzyme and keeping their place on the microparticle surface. These observations are very interesting since new and different architectures

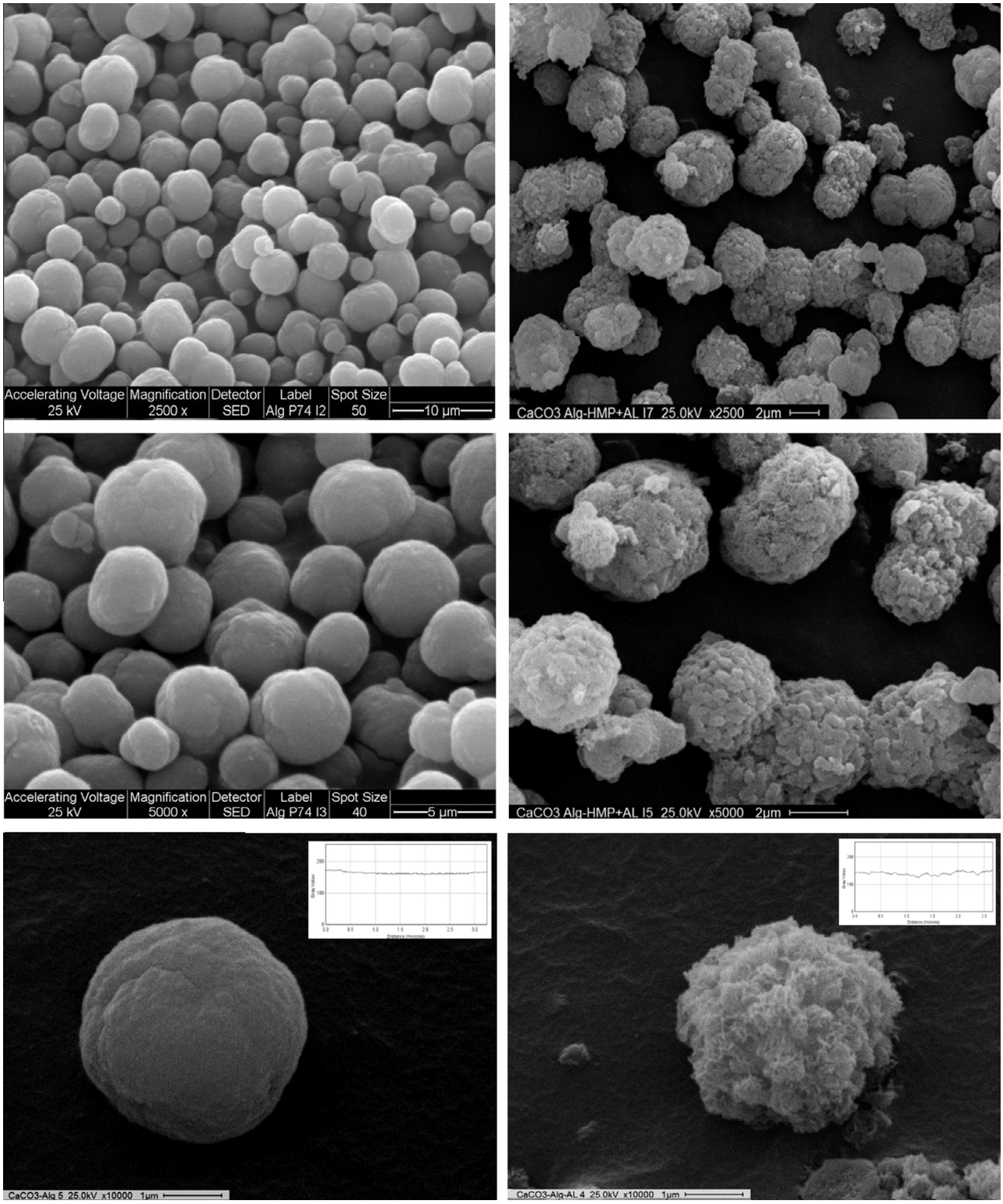

Fig. 4. SEM images of $CaCO_3$/Alg- High methoxyl Pectin microparticles at 2500× (up), 5000× (middle) and 10,000× (below) magnifications. Left: no treated. Right: Alginate Lyase treated microparticles. Some "nano-balloon" patterns are observed on surface. The plot profile of microsphere surface is shown in the corner of the bottom images.

can be produced on hybrid $CaCO_3$ particles, especially when a coacervate of two polymers were treated by specific enzyme able to hydrolyze only one of them. Controls were performed incubating hybrid microparticles in presence of phosphate buffer at 37 °C for 48 h and observed by SEM (ESI, Fig. 4S). Images revealed that microparticles maintained their structure and no changes on surface were observed, indicating that AL treatment is needed to develop the new architectures. Additionally, small peak of phosphorous was detected in the EDAX spectrum of the AL treated hybrid microparticles (ESI, Fig. 5S). The small quantity of apatite deposition on microparticles surface can be observed because of the poor solubility of phosphate in medium containing microparti-

cles with high calcium content and taken into account that the solubility of $Ca_3(PO_4)_2$ is very low ($K_{ps} = 2.07 \times 10^{-33}$).

SEM images were analyzed by ImageJ software in order to quantify the changes made by AL on microparticles surfaces. The plot profiles of the microparticles surface are shown in the insets of the Figs. 3 and 4. The $CaCO_3$/Alg microparticles showed a smooth plot profile, without significant differences in the gray values of the whole surface. It was reflected in the low standard deviation value. In contrast, the plot profile showed a rougher surface pattern and an increase of the standard deviation from 15 to 23 of $CaCO_3$/Alg microparticles treated with AL. As previously reported, it was demonstrated that "the less the standard variation value is, the smoother the surface is" [32]. As it was expected, $CaCO_3$/Alg–HMP microparticles showed also a smooth plot profile, which drastically changed after AL treatment. The standard deviation was increased from 22 to 27, revealing more differences in the height of the surface patterns (which means more differences in the gray values). However, it was a clear difference between the plot profiles of both treated matrices. The $CaCO_3$/Alg microparticles treated with AL showed peaks around 50 nm, meanwhile the $CaCO_3$/Alg–HMP microparticles AL treated exhibited the previously called "nano-balloon" patterns in the range of 200–500 nm.

The size distribution of microparticles was established in order to determine if they are acceptable for lung delivery (Fig. 5). The $CaCO_3$/Alg microparticles showed a mean diameter of 4.6 ± 0.7 μm, but the AL treated $CaCO_3$/Alg microparticles displayed a reduction of the mean size to 3.6 ± 0.5 μm. The size reduction of 1.0 μm (≈22%) can be attributed to the biopolymer hydrolysis after enzymatic alginate depolymerization. On the other side, $CaCO_3$/Alg–HMP microparticles exhibited a mean size of 4.0 ± 0.8 μm and 3.6 ± 0.4 μm before and after AL treatment respectively which is representing about 10% of decrease in the particle size. Besides, all tested microparticles were in the order of the 5 μm, which is the ideal size for pulmonary delivery as previously reported [4].

The porosity of the hybrid microparticles were also characterized by nitrogen adsorption isotherms (Table 2; ESI, Fig. 6S). This powerful technique can allow to establish the crucial role of AL in creating larger and new pores [33]. Calcium carbonate microparticles showed a surface area of 16.4 m^2 per gram of sample. When in both cases, alginate and alginate/HMP were added to the formulation, an increase in the surface area of 3 and 2 times respectively was found. The increase of microparticles surface produced by the biopolymers can be explained considering that biopolymer gels can provide a new internal network into the $CaCO_3$ structure with a high surface to volume ration. Also, it was interesting to analyze the reduction in the $CaCO_3$ pore size (calculated from both BJH and BET equations) from 32 nm to 6 and 11 nm for $CaCO_3$/Alg and $CaCO_3$/Alg–HMP microparticles respectively. In addition, a reduction in the pore volume was observed. These results are suggesting that biopolymers added to the formulation are incorporated by filling the original pores of the $CaCO_3$ matrix. Also, changes in pore size of hybrid particles treated with AL were confirmed by this method (Table 2). $CaCO_3$/Alg microparticles treated with AL showed 50% increase in surface area compared with no treated microparticles. The pore volume was increase 3 times and the pore size after AL hydrolysis was at least twice. The same tendency was observed for $CaCO_3$/Alg–HMP microparticles. After treatment, the surface area was increase in a 100%, the pore volume was at least twice and 3 nm increases in pore size was observed. All these changes reflect the effect of the enzymatic activity over the surface of the matrices, creating a new architecture more porous, because of the removal of alginate chains from the hybrid calcium carbonate structure.

By this methodology is possible to conclude that the microstructure of the porous can be changed by the chemical composition and the physicochemical environmental conditions. The chemical composition can be modified by: (1) the concentra-

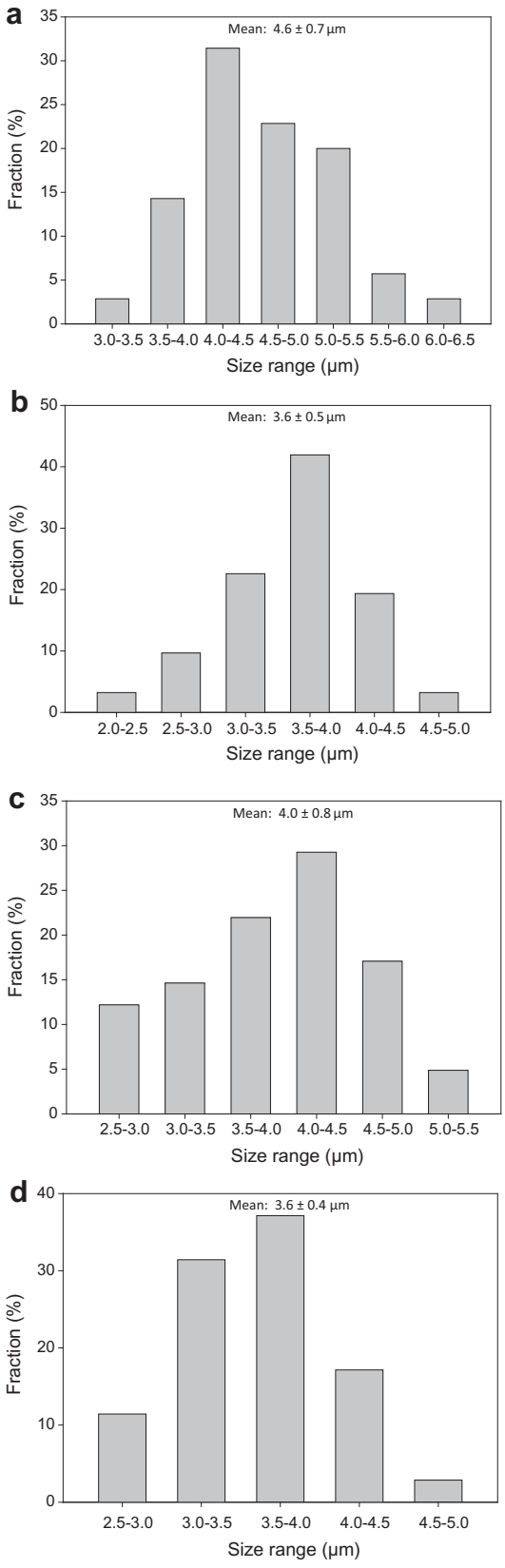

Fig. 5. Size distribution of microparticles. The mean diameter of each microparticle is mentioned at the top. (a) $CaCO_3$/Alg; (b) $CaCO_3$/Alg treated with AL; (c) $CaCO_3$/Alg–HMP; (d) $CaCO_3$/Alg–HMP treated with AL.

Table 2
Characterization of microparticles by nitrogen adsorption isotherms (BET).

Sample	Surface area (m^2/g)	Pore volumen (cm^3/g)[a]	Pore size (nm)	
			BJH adsorption	BET method
$CaCO_3$	16.4	0.13	32.5	31.1
$CaCO_3$/Alg	51.4	0.08	6.1	6.5
$CaCO_3$/Alg + AL	74.9	0.25	13.0	13.2
$CaCO_3$/Alg–HMP	34.9	0.09	11.0	10.8
$CaCO_3$/Alg–HMP + AL	71.6	0.24	13.5	13.3

In all cases standard deviation is less than 5.0%.
[a] BJH Adsorption cumulative volume of pores between 1.700 nm and 300.000 nm width.

tion of the pectin–alginate coacervate during the particle synthesis; (2) the ratio between pectin and alginate in the coacervate, (3) the concentration of alginate lyase. Furthermore, the environmental conditions such as pH, temperature and ionic strength can modify the gelling conditions as well as the partial degradation of alginate by the enzyme.

3.3. Levofloxacin loading and release from microparticles

Levofloxacin (Levo) was incorporated into microparticles by absorption mechanism. The loading efficiency of the different formulations and the drug/matrix mass ration are shown in Table 3. The hybrid $CaCO_3$ microparticles incorporated a low amount of the antibiotic. Hybrid $CaCO_3$/Alg loaded a 13.5% of the initial Levo, meanwhile the $CaCO_3$/Alg–HMP only loaded a 5.8%. The last result was contradictory with the previous reports of our laboratory showing interactions higher than 25% between other members of fluoroquinolone family, e.g. enrofloxacin and ciprofloxacin, in the presence of HMP [10,34]. However, the low incorporation of Levo into the hybrid $CaCO_3$ Alg–HMP matrix could be explained considering the synergistic interaction between alginate and high methoxyl pectin chains [35], which are restricting the available sites for Levofloxacin binding. Nevertheless, after AL treatment, the Levofloxacin absorption into the microparticles was increased in 3 and 9 times for $CaCO_3$/Alg and $CaCO_3$/Alg–HMP respectively.

The increase of the antibiotic adsorption on treated microspheres could be justified based on two considerations. The first one involves the adsorption of the antibiotic into a structure with a higher area to volume ratio and especially on naked surface areas of the $CaCO_3$ particles created by the hydrolysis of alginate chains made by the alginate lyase. But also, the hydrolysis of alginate by the enzymatic treatment on the microsphere surface is generating "biopolymeric hairy structures" (observed by SEM) in where the hydrolyzed polymer kept in the microparticle surface was partially free creating a corolla of alginate and pectin chains able to bind the fluoroquinolone. This hypothesis is based on previous results of our group, in where the ciprofloxacin, a fluoroquinolone structurally related to Levofloxacin, binds alginate, pectins and their coacervates in solution [10]. Additionally, the Levofloxacin as a member of the fluoroquinolones has the particular ability to stack among them [37]. In this sense, the raise in Levofloxacin concentration in the microparticles could be enhanced by the Π-stacking, reason why the mass loading is much larger than the increase in the surface area.

In order to corroborate the increase in Levofloxacin absorption and the drug localization inside microparticles, optical and epifluorescence microscopies were carried out (Fig. 6). Calcium carbonate microparticles without Levo showed no fluorescence under UV-light. However, the presence of biopolymers (alginate and Alg–HMP) into hybrid microparticles produced a slight fluorescence background. For this reason, the exposition time of the digitizer was adjusted to obtain cero fluorescence intensity for images of no Levo loaded microparticles. Maintaining all the visual parameters constant, $CaCO_3$/Alg (Levo) microparticles were observed. As it is shown in Fig. 6b, microparticles showed the typical fluorescence associated with the presence of Levo and the antibiotic was strictly located inside microparticles. When AL treated microparticles were observed under the same optical conditions, a significant increase in microparticles fluorescence was found,

Table 3
Levofloxacin loading into microparticles by absorption.

Microparticle sample	Loading efficiency (%)	Levofloxacin/matrix ratio (μg/mg)
$CaCO_3$/Alg	13.5 ± 2.1	4.3 ± 0.7
$CaCO_3$/Alg–HMP	5.8 ± 1.4	1.8 ± 0.4
$CaCO_3$/Alg + AL	38.1 ± 0.3	12.1 ± 0.1
$CaCO_3$/Alg–HMP + AL	43.4 ± 1.4	14.0 ± 0.6

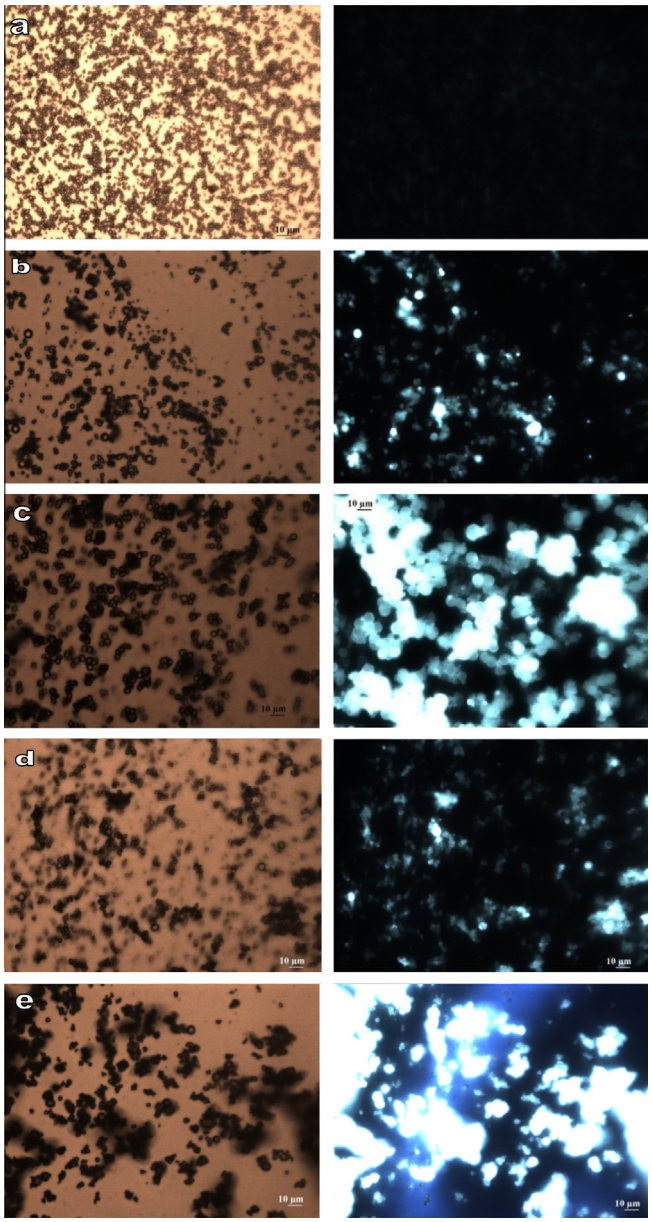

Fig. 6. Optical microscopy at visible (left) and UV (right) lights of microparticles: (a) $CaCO_3$ (empty); (b) $CaCO_3$/Alg (Levo); (c) $CaCO_3$/Alg + AL (Levo); (d) $CaCO_3$/Alg–HMP (Levo); (e) $CaCO_3$/Alg–HMP + AL (Levo).

correlated to higher Levo content. In a similar way, the fluorescence of control $CaCO_3$/Alg–HMP no loaded microparticles was adjusted to cero. After that, Levofloxacin loaded microparticles were observed, specific antibiotic localization into microparticles was found and a remarkable increase in fluorescence in AL treated ones (until signal saturation). These results were in concordance with the previous results of Levo loading exposed in Table 3.

When the hybrid microparticles were incubated in the release media, different Levo release profiles were found (Fig. 7). Besides the consideration of Levofloxacin as water soluble drug, the antibiotic showed a slow release from microparticles to the bulk solution probably because the drug strongly interacts with the polymers chains, similarly as it was previously reported in a recent work for ciprofloxacin and alginate–HMP coacervates [10]. The $CaCO_3$/Alg microparticles released the total content of Levofloxacin in 24 h, characterized by a burst release in the first 6 h followed by a slow release stage. After AL treatment, the release percentage was reduced and microparticles release the 60% of the initial drug in 24 h, which represents a 7.5 μg of Levo per milligram of vehicle (Fig. 7a). This change could be attributed to the increase of Levo loading after AL treatment, which leads to a more stackable drug structure inside the matrix and a consequent slow diffusion outside of the microparticle [36]. Additionally, the free chains of alginate produced by AL treatment were covering the surface of the particles like a corolla and would be able to bind the fluoroquinolone [10].

On the other hand, the strong interaction of HMP with fluoroquinolones was reflected in the release profile of $CaCO_3$/Alg–HMP microparticles. Levofloxacin was 20% released in the first 6 h, but a few amount of drug was release in the next 18 h (less than 0.1 μg of Levo per milligram of vehicle), possibly due, to its binding with HMP. However, after AL treatment, the microparticles exhibited an increase in the surface area and the drug was more susceptible to be detached from HMP, and consequently, the drug continuous being released after the first 6 h (Fig. 7b). Also, a lower amount of alginate chains were hydrolyzed by the enzyme, meanwhile HMPectin remains gelled on the microparticle surface, and consequently, low amount of free alginate chains were able to bind the antibiotic, reason why the Levo release percentage was higher than no treated microparticles. This result is relevant because provides a powerful tool to modify and control the release patterns of the device, regulating the drug doses needed to fit the therapeutic window by controlling polymer content and composition.

3.4. Microbiological assay

The antimicrobial capacity of microparticles was tested against *P. aeruginosa* ATCC 15442 (Fig. 8), a common recurrent and opportunistic pathogen of lung infections, affecting patients with HIV and a weak or depressed immune system, patients with lung cancer and also with genetic disorders like Cystic Fibrosis [37–39]. Controls of both, only bacteria and in presence of empty micropar-

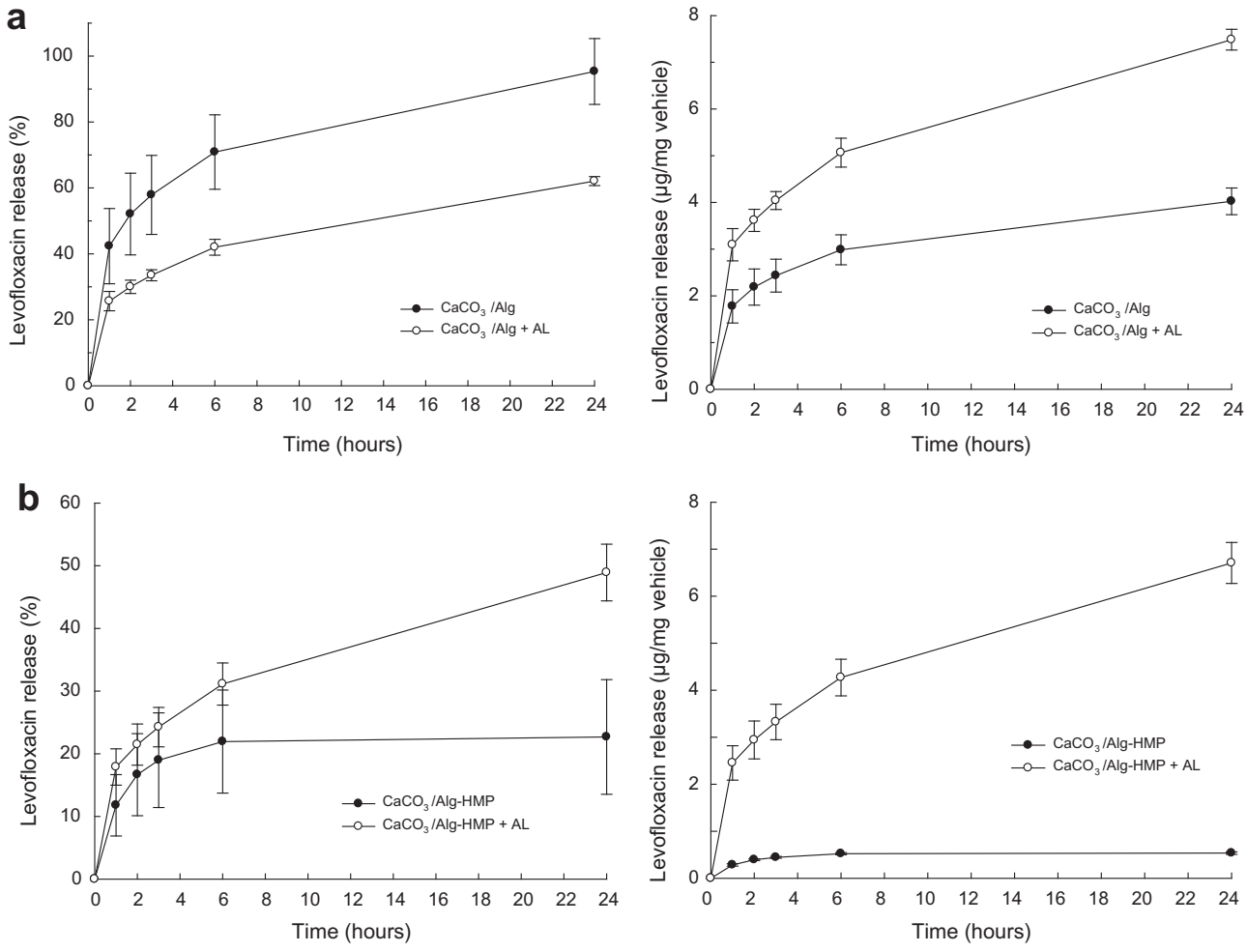

Fig. 7. Kinetic release of Levofloxacin from (a) $CaCO_3$/Alg microparticles and (b) CaCO3/Alg–HMP. The effect on release after AL treatment was observed in both matrices. Left: release percentage. Right: mass of Levo per mass of vehicle.

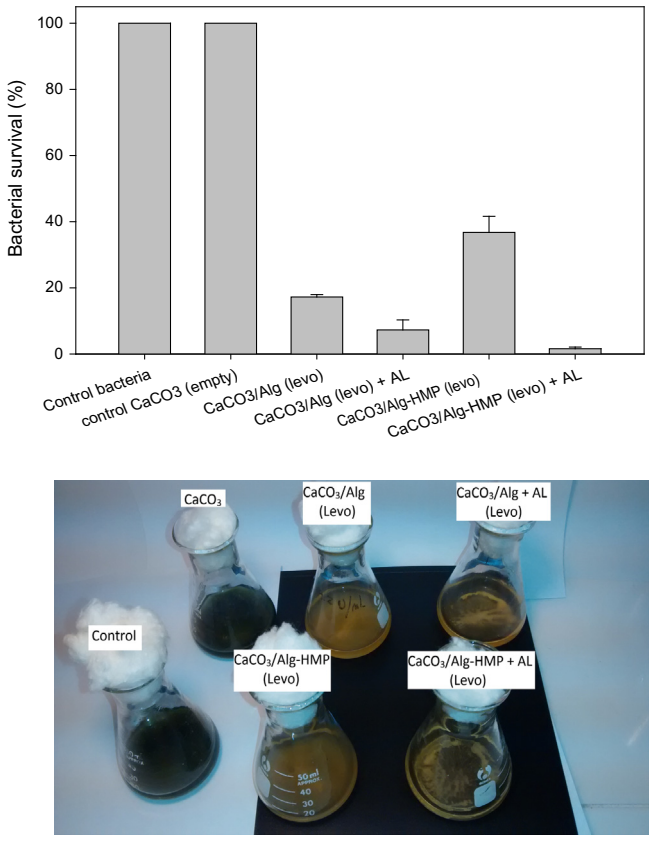

Fig. 8. Antimicrobial assay of microparticles against *Pseudomonas aeruginosa* after 24 h incubation.

ticles, showed an intense growth after 24 h incubation, with an exacerbate increase of viscosity associated to the biopolymer production, and green color because of the fluorescent pigments. When Levofloxacin loaded microparticles (both $CaCO_3$/Alg and $CaCO_3$/Alg–HMP) were incorporated into the flask containing the bacteria growing at exponential phase in nutrient broth, a partial inhibition was observed. The decrease of viscosity in the medium indicates the reduction or absence of biopolymer production, which means that the bacteria were not capable to reach the stationary phase. $CaCO_3$/Alg produced a higher inhibition than $CaCO_3$/Alg–HMP microparticles, due to their higher loading and the burst release. More interesting, when AL treated microparticles containing Levo were incubated with the bacteria, a higher inhibition was found after 24 h. Moreover, no viscosity changes were observed in the microbial culture suggesting a strong depletion of biopolymeric production which is commonly associated with high pathogenicity of the strain. The microbial culture inhibition was mainly produced because of the higher loading efficiency of AL treated microparticles, and the capability to release more amount of antibiotic and reach the minimum inhibitory concentration of *P. aeruginosa*. These results were correlated with a control experiment of bacterial survival at increasing concentrations of free Levo (Fig. 7S). The bacteria were fully inhibited at Levo concentration higher than 3.0 μg/ml. Taking into the account that the percentages of bacterial survival for the different microparticles, it was found that the $CaCO_3$/Alg and $CaCO_3$/Alg–HMP formulations released the 100% of the antibiotic content, while the AL treated ones released around 55%. These results are in agreement with the release profiles obtained in PBS solution at pH = 7.0, with the exception of the $CaCO_3$/Alg–HMP microparticles, which was expected to release less than 20% of the Levofloxacin. This discrepancy can be attributed to the changes in the release media (bacteria were growing in a nutrient broth) affecting the stability of the formulation and therefore increased the release profile.

The presented results are confirming the therapeutic relevance of AL modification on the hybrid particles, enhancing the drug absorption, providing a controlled release profile and showing inhibitory effects against *P. aeruginosa.*

4. Conclusions

The present work proposes a new method for the synthesis of tailorable hybrid $CaCO_3$–biopolymer microparticles with novel architectures. Microparticles with 5 μm diameter size containing nanoporous were developed. The increase in the surface area after treatment allowed the incorporating an antibiotic model (Levofloxacin) by absorption with high loading efficiency. Controlled release properties of the matrix are providing a sustainable drug administration on time. The modifications of the matrices were confirmed by analysis of total carbohydrates content, DSC, FTIR, XRD, Nitrogen adsorption isotherms, SEM, EDAX, optical and epi-fluorescence microscopies. Enzymatically treated microparticles showed an enhanced antimicrobial effect against an opportunistic pathogen, *P. aeruginosa*.

Results are indicating the developed of a new architecture of $CaCO_3$ hybrid microparticles, with a valuable application in the adsorption of drugs and potentially extended to other therapeutic molecules with biological activity. In this sense, the limitations of the $CaCO_3$ matrices are overcome with the present enzymatic modification [8].

A new application of Alginate Lyase activity was found as a tailoring tool for alginate gels and alginate gel coacervates. In the present work, AL was not only capable to be active on gelled alginate [17], but also the hydrolysis of alginate chain present on hybrid matrices was demonstrated. In this sense, the biocatalyst recognizes the specific regions compose of the biopolymer hybridized with an inorganic phase, and particularly, with precise targeting to alginate, even in presence of pectin. Additionally, the tailoring of $CaCO_3$ hybrid microparticles can be performed by modifying the amount and ratio of alginate–HMPectin during particle synthesis and also by changing the environmental conditions that directly affect the enzymatic activity of AL. These characteristics allow to modulate the properties of the microparticles in terms of hydrophilicity/hydrophobicity, and correlate them with the properties of the cargo molecules, the time and profile of drug loading and kinetic release required to reach therapeutic doses. As far as we know, this is the first report of an alginate lyase acting on a hybrid organic/inorganic matrix.

Finally, the capability of treated microparticles to be inhaled is currently tested *in vivo*. Experiments with model mice and rats inhaling the microparticles are in course in order to establish the effectiveness of microparticles to reach the deepest interstices of lung.

Acknowledgments

We want to special thank Dr. Jimena González for her kind support and expertise in DSC, XRD and FTIR studies and Prof. Vera Alvarez for allowing to use the facilities and equipment of The Institute of Research in Science and Technology of Materials (INTEMA, CONICET, Mar del Plata, Argentina). The present work was supported by Argentine grants from CONICET (National Council for Science and Technology, PIP 0214), The National Agency of Scientific and Technological Promotion (ANPCyT, PICT 2011-2116), *Fundación Argentina de Nanotecnología* and UNLP (National University of La Plata, 11/X545 and PRH 5.2).

Appendix A. Supplementary material

Kinetic degradation of hybrid microparticles by AL; DSC curves of microparticles; SEM images of microparticles at 500 magnifications; SEM images of control microparticles incubated in phosphate buffer without AL treatment; Energy Dispersive X-ray analysis of control microparticles; nitrogen adsorption isotherms of the different microparticles. Supplementary data associated with this article can be found, in the online version, at http://dx.doi.org/10.1016/j.jcis.2014.10.007.

References

[1] T. Beuvier, B. Calvignac, G.J.R. Delcroix, M.K. Tran, S. Kodjikian, N. Delorme, J.F. Bardeau, A. Gibaud, F. Boury, J. Mater. Chem. 21 (2011) 9757.
[2] C.Y. Peng, Q.H. Zhao, C.Y. Gao, Colloids Surf. A Physicochem. Eng. Asp. 353 (2010) 132.
[3] F. Ishikawa, M. Murano, M. Hiraishi, T. Yamaguchi, I. Tamai, A. Tsuji, Pharm. Res. 19 (2002) 1097.
[4] Y. Cai, Y. Chen, X. Hong, Z. Liu, W. Yuan, Int. J. Nanomed. 8 (2013) 1111.
[5] D.E. Geller, P.A. Flume, D.C. Griffith, E. Morgan, D. White, J.S. Loutit, M.N. Dudley, Antimicrob. Agents Chemother. 55 (2011) 2636.
[6] A. Yanagawa, T. Kudo, Y. Mizushima, Jpn. J. Clin. Pharmacol. Ther. 26 (1995) 127.
[7] S. Haruta, T. Hanafusa, H. Fukase, H. Miyajima, T. Oki, Diabetes Technol. Ther. 5 (2003) 1.
[8] Y. Ueno, H. Futagawa, Y. Takagi, A. Ueno, Y. Mizushima, J. Control Rel. 103 (2005) 93.
[9] M. Díaz-Dosque, P. Aranda, M. Darder, J. Retuert, M. Yazdani-Pedram, J. Luis Arias, E. Ruiz-Hitzky, J. Cryst. Growth 310 (2008) 5331.
[10] G.A. Islan, I. Perez de Verti, S.G. Marchetti, G.R. Castro, Appl. Biochem. Biotechnol. 167 (2012) 1408.
[11] V.E. Bosio, V. Machain, I. Pérez De Berti, A. Gómez López, S.G. Marchetti, M. Mechetti, G.R. Castro, Appl. Biochem. Biotechnol. 167 (2012) 1365.
[12] S.K. Bajpai, S. Sharma, React. Funct. Polym. 59 (2004) 129.
[13] I. Braccini, S. Pérez, Biomacromolecules 2 (1995) 1089.
[14] M.C. Klak, E. Lefebvre, L. Rémy, R. Agniel, J. Picard, S. Giraudier, V. Larreta-Garde, Macromol. Biosci. 13 (2013) 687.
[15] G.A. Islan, V.E. Bosio, G.R. Castro, Macromol. Biosci. 13 (2013) 1238.
[16] T.Y. Wong, L.A. Preston, N.L. Schiller, Annu. Rev. Microbiol. 54 (2000) 289.
[17] V. Breguet, U.V. Stockar, I.W. Marison, Biotechnol. Prog. 23 (2007) 1223.
[18] C. Carbon, Chemotherapy 47 (2001) 9.
[19] E. Rubinstein, Chemotherapy 47 (2001) 3.
[20] V.E. Bosio, M.L. Cacicedo, B. Calvignac, I. León, T. Beuvier, F. Boury, G.R. Castro, Colloids Surf. B: Biointerfaces (2014), http://dx.doi.org/10.1016/j.colsurfb.2014.09.011.
[21] J.F. Preston III, J.D. Rice, M.C. Chow, B.J. Brown, Carbohyd. Res. 215 (1991) 147.
[22] E.W. Yemm, A.J. Willis, Biochem J. 57 (1954) 508.
[23] W.G.T. Willats, J.P. Knox, J.D. Mikkelsen, Trends Food Sci. Technol. 17 (2006) 97.
[24] A.V. Radha, T.Z. Forbes, C.E. Killian, P.U.P.A. Gilbert, A. Navrotsky, PNASS (USA) 107 (2010) 16438.
[25] A.C. Tas, Use of vaterite and calcite in forming calcium phosphate cement scaffolds, in: M. Brito, E. Case, W.E. Kriven, J. Salem, D. Zhu (Eds.), Porous, Biological and Geopolymer Ceramics: Ceramic Engineering and Science Proceedings, 28, Wiley and Sons, 2009, p. 135, http://dx.doi.org/10.1002/9780470339749.
[26] Y.Y. Kim, A.S. Schenk, J. Ihli, A.N. Kulak, N.B. Hetherington, C.C. Tang, et al., Nat. Commun. 5 (2014) 1, http://dx.doi.org/10.1038/ncomms5341.
[27] B.V. Parakhonskiy, A.M. Yashchenok, S. Donatan, D.V. Volodkin, F. Tessarolo, R. Antolini, et al., ChemPhysChem 15 (2014) 2817.
[28] K. Sakugawa, A. Ikeda, A. Takemura, H. Ono, J. Appl. Polym. Sci. 93 (2004) 1372.
[29] C.C. Ribeiro, C.C. Barriasa, M.A. Barbosa, Biomaterials 25 (2004) 4363.
[30] H.P. Erickson, Size and shape of protein molecules at the nanometer level determined by sedimentation, gel filtration, and electron microscopy, in: Shulin Li (Ed.), Biological Procedures Online, 11, Springer-Verlag, 2009, p. 32. http://dx.doi.org/10.1007/s12575-009-9008-x.
[31] M.L. Garron, M. Cygler, Glycobiology 20 (2010) 1547.
[32] Y.W. Wang, Q. Wu, G.Q. Chen, Biomacromolecules 6 (2005) 566.
[33] K. Sing, Colloids Surf. A Physicochem. Eng. Asp. 187–188 (2001) 3.
[34] Y.N. Martínez, L. Piñuel, G.R. Castro, J.D. Breccia, Appl. Biochem. Biotechnol. 167 (2012) 1421.
[35] P. Walkenström, S. Kidman, A.M. Hermansson, P.B. Rasmussen, L. Hoegh, Food Hydrocol. 17 (2003) 593.
[36] N. Maurer, K.F. Wong, M.J. Hope, P.R. Cullis, Biochim. Biophys. Acta (BBA)-Biomembr. 1374 (1998) 9.
[37] D.H. Dockrell, R. Breen, M. Lipman, R.F. Miller, HIV Med. (2011) 12.
[38] J.C. Ruckdeschel, J. Greene, K.E. Sommers, K.K. Fields, in: D.W. Kufe, R.E. Pollock, R.R. Weichselbaum, et al. (Eds.), Respiratory Infections in Patients with Cancer in Holland-Frei Cancer Medicine, sixth ed., BC Decker, Canada, 2003.
[39] N. Høiby, O. Ciofu, T. Bjarnsholt, Future Microbiol. 5 (2010) 1663.